

HYDRODYNAMIC APPROACH TO RELATIVISTIC HEAVY ION COLLISIONS*

TETSUFUMI HIRANO

Department of Physics, Sophia University, Tokyo 102-8554, Japan
and

Department of Physics, University of Tokyo, Tokyo 113-0033, Japan

(Received October 14, 2011)

We analyze the elliptic flow parameter v_2 in Pb+Pb collisions at the LHC energy using a hybrid model in which the evolution of the quark-gluon plasma is described by ideal hydrodynamics and the subsequent hadronic stage by a hadron cascade model. For initial conditions, we employ Monte Carlo versions of the Glauber and the Kharzeev–Levin–Nardi models and compare results with each other. We demonstrate that the differential elliptic flow $v_2(p_T)$ does not change so much when the collision energy increases, whereas the integrated v_2 increases due to the enhancement of mean transverse momentum.

DOI:10.5506/APhysPolB.42.2811

PACS numbers: 25.75.-q, 25.75.Nq, 12.38.Mh, 12.38.Qk

1. Introduction

Heavy ion programs at Large Hadron Collider (LHC) in CERN and at Relativistic Heavy Ion Collider (RHIC) in Brookhaven National Laboratory provide us a unique opportunity to explore novel deconfined matter, the quark-gluon plasma (QGP).

Relativistic hydrodynamics is one of the successful frameworks to describe space-time evolution of the QGP in relativistic heavy ion collisions. Elliptic flow [1], which played an essential role to establish a new paradigm of the strongly coupled QGP [2,3] at RHIC [4], is one of the key observables to investigate the bulk and transport properties of the QGP. First elliptic flow data in Pb+Pb collisions at $\sqrt{s_{NN}} = 2.76$ TeV were recently published by the ALICE Collaboration [5] followed by the ATLAS Collaboration [6].

* Presented at the LI Cracow School of Theoretical Physics “Soft Side of the LHC”, Zakopane, Poland, June 11–19, 2011.

The first goal of flow measurements is to see whether hydrodynamic models reproduce the flow as well at LHC as at RHIC and thus whether the QGP depicts similar strong coupling nature at LHC.

Since the matter created in heavy ion collisions would reach a locally equilibrated state at most only in the intermediate stage where hydrodynamic description is expected to work, one needs to model the initial stage and the final stage of the whole reaction using other dynamical approaches. In this paper, we show results from a hybrid modeling of the whole stage including Monte Carlo approaches to initial conditions, ideal hydrodynamic description of the QGP and kinetic description of the hadron gas.

2. The model

We calculate the elliptic flow parameter v_2 at midrapidity and its transverse momentum (p_T) dependence in Pb+Pb collisions at LHC and compare them with the data [7, 8]. The expansion of the QGP is described by ideal hydrodynamics [9] and the subsequent evolution of hadronic matter below switching temperature $T_{sw} = 155$ MeV, is described using a hadronic cascade model JAM [10].

During the fluid dynamical stage, we solve relativistic hydrodynamic equations

$$\partial_\mu T^{\mu\nu}(x) = 0 \quad (1)$$

with an assumption of ideal hydrodynamic decomposition of energy momentum tensor

$$T^{\mu\nu} = eu^\mu u^\nu - P(g^{\mu\nu} - u^\mu u^\nu), \quad (2)$$

where e , P and u^μ are energy density, pressure and four flow velocity, respectively. For the equation of state, $P = P(e)$, we employ EoS *s95p-v1.1*, which interpolates between hadron resonance gas at low temperature and recent lattice QCD results by the hotQCD Collaboration [11, 12] at high temperature in the same way as *s95p-v1* [13], but the hadron resonance gas part contains the same hadrons and resonances as the JAM hadron cascade [10]. Details of the interpolating procedure are explained in Ref. [13] and the parametrization and EoS tables are available at Ref. [14]. Below the switching temperature T_{sw} , we describe the space-time evolution of the hadron resonance gas by using a hadronic cascade model JAM [10]. Kinetic freezeout happens gradually in the kinetic approaches contrary to the conventional fluid dynamical approach using the Cooper–Frye formula [15] which describes a unrealistic sudden freezeout at a freezeout hypersurface. Hadronic cascade models have also other advantage over hydrodynamic approaches to hadronic viscous fluids when one discusses hadronic species dependent phenomenon such as violation of mass ordering pattern in differential elliptic flow [16].

Initial time of hydrodynamic simulations is fixed to be $\tau_0 = 0.6$ fm/ c throughout this work. For initial conditions in the longitudinal direction, we assume the Bjorken scaling solution [17]. To initialize the density distributions in the transverse plane, we utilize two Monte Carlo approaches: Monte Carlo Glauber (MC-Glauber) model [18] and Monte Carlo Kharzeev–Levin–Nardi (MC-KLN) model [19]. Using these Monte Carlo models, we calculated initial conditions for hydrodynamic simulations in the transverse plane with respect to participant plane and reaction plane [20]. Initial density profiles with respect to participant plane contain effects of eccentricity fluctuation on average. However, the ALICE Collaboration mainly obtained v_2 using the 4-particle cumulant method $v_2\{4\}$ [21]. If the event-by-event distribution of eccentricity in the reaction plane was a two-dimensional Gaussian and if v_2 was proportional to the participant eccentricity, $v_2\{4\}$ yields the value of v_2 in the reaction plane [22, 23]. Therefore, we calculate initial profiles with respect to the reaction plane when we compare our results with experimental data from the ALICE Collaboration: We average over many events using Monte Carlo calculations instead of shifting and rotating a distribution event-by-event to match the main and sub axes of the ellipsoids as was done in the previous work [7, 20]. It should be noted that the distributions obtained in this way are not identical to the ones from the optical Glauber model or the factorized KLN (fKLN) model [24] due to finite nucleon size effects [19, 25]: Collision points in the transverse plane are smeared using inelastic cross-section of $p + p$ collisions in the “mean-field” option in the Monte Carlo approach [19] to obtain smooth initial conditions for hydrodynamic simulations.

In the MC-KLN model, we calculate distribution of gluons at each transverse grid using the k_t -factorized formula [26]. Using the thickness function T_A , we parametrize the saturation scale for a nucleus A as

$$Q_{s,A}^2(x; \mathbf{x}_\perp) = Q_{s0}^2 \frac{T_A(\mathbf{x}_\perp)}{T_{A0}} \left(\frac{x_0}{x}\right)^\lambda, \quad (3)$$

where $T_{A0} = 1.53$ fm $^{-2}$, $x_0 = 0.01$ and $Q_{s0}^2 = 2$ GeV 2 . We choose $\lambda = 0.28$ and a proportionality constant in the unintegrated gluon distribution in the k_t -factorized formula to reproduce centrality dependence of p_T spectra obtained by the PHENIX Collaboration [27]. Thickness function at each transverse coordinate is obtained by counting the number of wounded nucleons N within a tube extending in the beam direction with radius $r = \sqrt{\sigma_{NN}^{\text{in}}/\pi}$ from each grid point

$$T_A(\mathbf{x}_\perp) = \frac{N}{\sigma_{NN}^{\text{in}}}. \quad (4)$$

For each generated configuration of nucleons in colliding nuclei, the k_T -factorization formula is applied at each transverse coordinate to obtain the distribution of produced gluons locally. We apply the Kharzeev–Levin–Nardi (KLN) approach [26] in the version previously employed in [28]. In this approach, the distribution of gluons at each transverse coordinate \mathbf{x}_\perp produced with rapidity y is given by the k_T -factorization formula [29]

$$\begin{aligned} \frac{dN_g}{d^2x_\perp dy} &= \frac{2\pi^2}{C_F} \int \frac{d^2p_T}{p_T^2} \int^{p_T} \frac{d^2k_T}{4} \alpha_s(Q^2) \\ &\quad \times \phi_A(x_1, (\mathbf{p}_T + \mathbf{k}_T)^2/4; \mathbf{x}_\perp) \\ &\quad \times \phi_B(x_2, (\mathbf{p}_T - \mathbf{k}_T)^2/4; \mathbf{x}_\perp), \end{aligned} \quad (5)$$

where $x_{1,2} = p_T \exp(\pm y)/\sqrt{s}$ and p_T is the transverse momentum of the produced gluons. We choose an upper limit of 10 GeV/ c for the p_T integration. For the unintegrated gluon distribution function we use

$$\phi_A(x, k_T^2; \mathbf{x}_\perp) = \frac{\kappa C_F (1-x)^4}{2\pi^3} \frac{Q_s^2}{\alpha_s(Q_s^2) \max(Q_s^2, k_T^2)}, \quad (6)$$

where $C_F = (N_c^2 - 1)/(2N_c)$. The parameter $\kappa^2 = 1.75$ is again chosen for the overall normalization of the gluon multiplicity in order to fit p_T spectra obtained by the PHENIX Collaboration [27]. As an initial condition for hydrodynamical calculations, the initial entropy density in the transverse plane is obtained by

$$s_0(\mathbf{x}_\perp) = 3.6n_g = 3.6 \left. \frac{dN_g}{\tau_0 d^2x_\perp d\eta_s} \right|_{y=\eta_s=0}. \quad (7)$$

Here, we identify gluon's momentum rapidity y with space-time rapidity η_s . As a default parameter set at LHC, we use the same parameters except for colliding energy and mass number of incident nuclei. This predicted $dN_{\text{ch}}/d\eta \sim 1600$ at 5% most central collisions [7], which turns out to be consistent with the recent ALICE measurement [30, 31].

In the MC-Glauber model, one calculates the number distributions of participants ρ_{part} and of binary collisions ρ_{coll} for a given nuclear density distribution. We model the initial entropy distribution in hydrodynamic simulations as a linear combination of ρ_{part} and ρ_{coll} in the transverse plane

$$\frac{dS}{\tau_0 d\eta_s d^2\mathbf{x}_\perp} = \frac{C}{\tau_0} \left(\frac{1-\alpha}{2} \rho_{\text{part}}(\mathbf{x}_\perp) + \alpha \rho_{\text{coll}}(\mathbf{x}_\perp) \right). \quad (8)$$

At the RHIC energy, the mixing parameter $\alpha = 0.18$ and the proportionality constant $C = 15.0$ in Eq. (8) are chosen to reproduce the centrality dependence of p_T spectra at RHIC [27]. We tune these two parameters in Pb+Pb collisions at LHC to reproduce the centrality dependence of charged hadron multiplicity [30]. For both initializations we do the centrality cuts according to the N_{part} distribution from the MC-Glauber model [7]

3. Results

We calculate $dN_{\text{ch}}/d\eta/(N_{\text{part}}/2)$ as a function of N_{part} for initial conditions from the MC-Glauber and the MC-KLN models and compare them with data in Fig. 1. The experimental data point in inelastic $p + p$ collisions at $\sqrt{s_{NN}} = 2.36$ TeV [32] is plotted at $N_{\text{part}} = 2$. The MC-KLN initialization leads to remarkable agreement with the ALICE data. On the other hand, it is difficult to fit the data within the current two-component picture in the MC-Glauber model: The results from the MC-Glauber initialization with $\alpha = 0.08$ and $C = 41.4$ almost trace the ones from the MC-KLN initialization and the ALICE data except for 0–5% and 70–80% centrality.

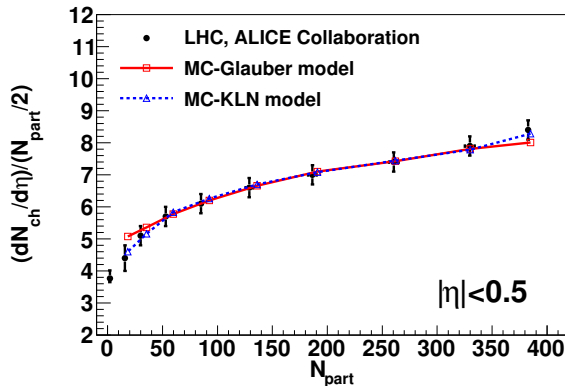


Fig. 1. Centrality dependences of charged hadron multiplicity in the MC-Glauber and the MC-KLN initialization are compared with ALICE data [30,32]. Each point in theoretical results from right to left corresponds to 0–5, 5–10, 10–20, 20–30, 30–40, 40–50, 50–60, 60–70 and 70–80% centrality, respectively.

Figure 2 shows the initial eccentricity with respect to reaction plane as a function of N_{part} in Pb+Pb collisions at $\sqrt{s_{NN}} = 2.76$ TeV and in Au+Au collisions at $\sqrt{s_{NN}} = 200$ GeV. As previously known, the k_t -factorized formula of KLN model generates larger eccentricity than the Glauber model does [24, 33]. In the MC-KLN model, eccentricity in Pb+Pb collisions at $\sqrt{s_{NN}} = 2.76$ TeV is slightly larger than that in Au+Au collisions at $\sqrt{s_{NN}} = 200$ GeV when the centrality is fixed [7]. On the other hand, in the

MC-Glauber model, eccentricity in Pb+Pb collisions at $\sqrt{s_{NN}} = 2.76$ TeV is slightly smaller than that in Au+Au collisions at $\sqrt{s_{NN}} = 200$ GeV for a fixed centrality. This is due to the smearing process we employed to obtain a smooth initial profile for hydrodynamic evolution. As mentioned, we use the inelastic cross-section in $p + p$ collisions, σ_{in} , to smear the distribution of collision points. This cross-section is ~ 1.5 times larger at LHC than at RHIC and thus the smearing area, $S = \sigma_{in}$ [19], is also larger at LHC and the eccentricity is reduced. Our smearing procedure also leads to a smaller eccentricity than the conventional value of MC-Glauber model. In the MC-Glauber model in the literature [18], one assumes δ function profile for each collision point in ρ_{part} distribution rather than a box-like profile in the present work. The effect of smearing is smaller in the MC-KLN initialization and we have checked that the eccentricity at LHC turns out to be essentially the same as at RHIC when the smearing area is the same.

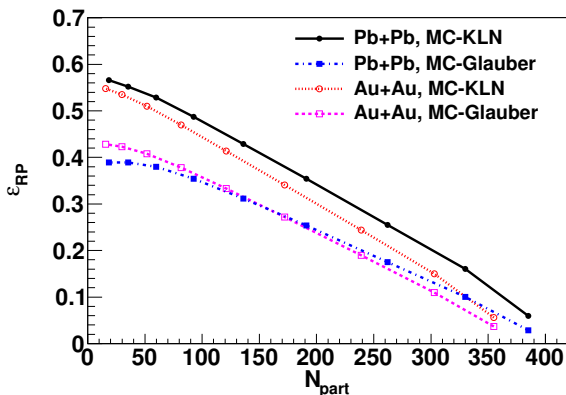


Fig. 2. Eccentricity with respect to the reaction plane as a function of N_{part} in Pb+Pb collisions at $\sqrt{s_{NN}} = 2.76$ TeV and in Au+Au collisions at $\sqrt{s_{NN}} = 200$ GeV. Each point from right to left corresponds to 0–5, 5–10, 10–20, 20–30, 30–40, 40–50, 50–60, 60–70 and 70–80% centrality, respectively.

Figure 3 shows comparison of transverse momentum distributions of charged hadrons between RHIC and LHC energies at 10–20% and 40–50% centralities. As clearly seen from figures, the slope of p_T spectra becomes flatter as collision energy and, consequently, pressure of produced matter increases. To quantify this, we calculate mean p_T of charged hadrons. In the MC-Glauber initialization, mean p_T increases from RHIC to LHC by 21% and 19% in 10–20% and 40–50% centrality, respectively. On the other hand, the corresponding fractions are 25% and 24% in the MC-KLN initialization. Since our calculations at RHIC were tuned to reproduce the p_T -spectra, this means that at LHC the spectra calculated using the MC-KLN initialization are slightly flatter than those calculated using the MC-Glauber initialization.

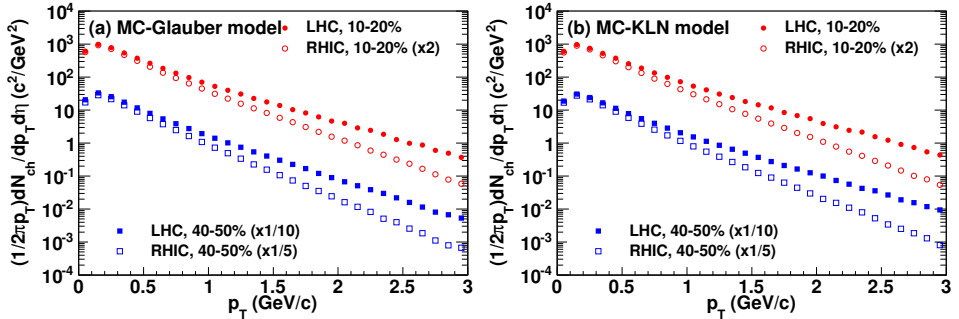


Fig. 3. Transverse momentum distribution of charged hadrons at 10–20% (circles) and 40–50% (squares) centralities in Pb+Pb collisions at $\sqrt{s_{NN}} = 2.76$ TeV (filled symbols) and in Au+Au collisions at $\sqrt{s_{NN}} = 200$ GeV (open symbols). Results from (a) the MC-Glauber initialization and (b) the MC-KLN initialization. For the sake of comparison and visibility, the spectra are scaled by 2, 1/10 and 1/5 for 10–20% at RHIC, 40–50% at LHC and 40–50% at RHIC, respectively.

We compare integrated v_2 for charged hadrons with respect to reaction plane with the ALICE [5] and STAR [34] $v_2\{4\}$ data in Fig. 4. When evaluating the integrated v_2 , we take account of both transverse momentum and pseudorapidity acceptance as done in the experiments, *i.e.* $0.2 < p_T < 5.0$ GeV/ c and $|\eta| < 0.8$ for ALICE, and $0.15 < p_T < 2.0$ GeV/ c and $|\eta| < 1.0$ for STAR. We emphasize that not only the p_T cut [35], but also the pseudorapidity cut plays an important role in a consistent comparison with the data. Due to the Jacobian for the change of variables from rapidity y to pseudorapidity η , $v_2(y = 0) < v_2(\eta = 0)$ for positive elliptic flow [36]. Notice that even if one assumes the Bjorken scaling solution, one has to consider the pseudorapidity acceptance since $v_2(\eta)$ is not constant even if $v_2(y)$ is [36]. In the case of the MC-Glauber (MC-KLN) initialization in 40–50% centrality, v_2 integrated over the whole p_T region is $\sim 14\%$ ($\sim 10\%$) larger at $\eta = 0$ than at $y = 0$.

When the MC-Glauber model is employed for initial profiles, centrality dependence of integrated v_2 from the hybrid approach almost agrees with both ALICE and STAR data. Since eccentricity fluctuation contributes little and negatively to $v_2\{4\}$ in non-Gaussian distribution of eccentricity fluctuation [22, 23], this indicates there is only little room for the QGP viscosity in the model calculation. On the other hand, apparent discrepancy between the results from the MC-KLN initialization and the ALICE and STAR data means that viscous corrections during the hydrodynamic evolution are required.

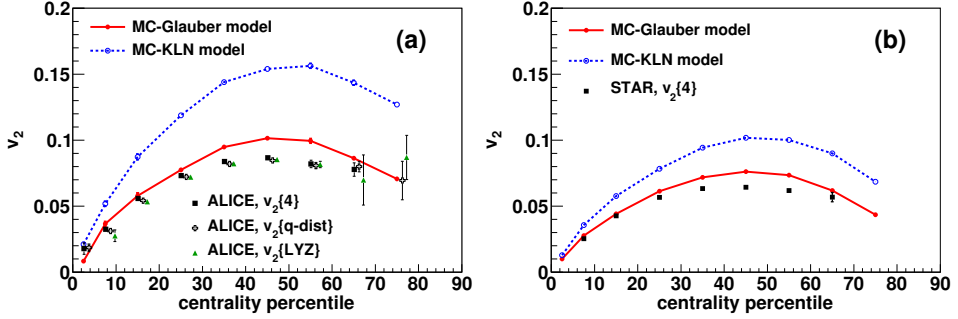


Fig. 4. Centrality dependences of v_2 for charged hadrons with respect to reaction plane (a) in Pb+Pb collisions at $\sqrt{s_{NN}} = 2.76$ TeV ($|\eta| < 0.8$, $0.2 < p_T < 5$ GeV/c) and (b) in Au+Au collisions at $\sqrt{s_{NN}} = 200$ GeV ($|\eta| < 1.0$, $0.15 < p_T < 2$ GeV/c) are compared with ALICE [5] and STAR [34] v_2 data, respectively. ALICE data points are shifted horizontally for visibility.

From RHIC to LHC, the p_T -integrated $v_2(|\eta| < 0.8)$ increases by 24% and 25% in 10–20% and 40–50% centrality, respectively, in the MC-Glauber initialization. On the other hand, in the MC-KLN initialization, the increase reaches 42% and 44% in 10–20% and 40–50% centrality, respectively. Since eccentricity does not change significantly (at most $\pm 6\%$ in 40–50% centrality) from RHIC to LHC as shown in Fig. 2, the significant increase of integrated v_2 must be attributed to a change in transverse dynamics.

Finally, we compare $v_2(p_T)$ of charged hadrons with ALICE [5] and STAR [34] data in 10–20% (Fig. 5(a)) and 40–50% (Fig. 5(b)) centrality. Interestingly, the data at LHC agree with the data at RHIC within errors. The calculated $v_2(p_T)$ shows similar independence of collision energy when

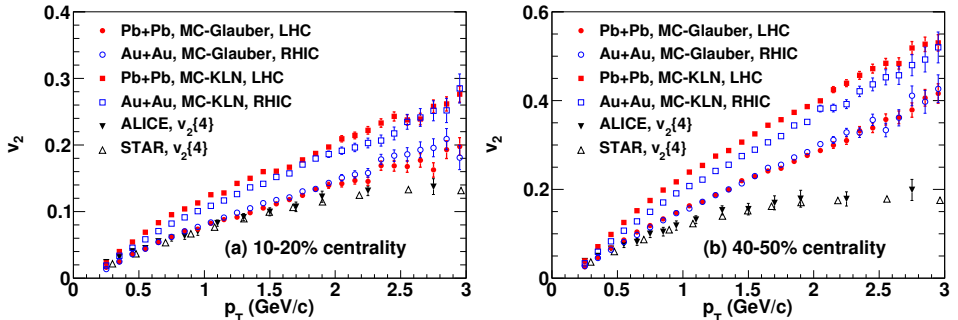


Fig. 5. Transverse momentum dependences of v_2 for charged hadrons in the MC-Glauber (circles) and the MC-KLN (squares) initialization are compared with ALICE [5] ($|\eta| < 0.8$, inverse triangles) and STAR [34] ($|\eta| < 1.0$, triangles) $v_2\{4\}$ data in (a) 10–20% centrality and (b) 40–50% centrality.

MC-Glauber initialization is used, whereas MC-KLN initialization leads to a slightly larger $v_2(p_T)$ at the larger energy. For MC-Glauber results, the fit to data is fair below $p_T \sim 1.5$ GeV/ c and $p_T \sim 0.8$ GeV/ c momenta in the 10–20% and 40–50% centralities, respectively. Results from the MC-KLN initialization at both energies are significantly larger than experimental data in the whole p_T region, which again indicates necessity of viscous corrections in hydrodynamic evolution. For both initializations the difference between the data and the calculated $v_2(p_T)$ is larger in more peripheral collisions. This too can be understood as an indication of viscosity, since the more peripheral the collision, the smaller the system and the more anisotropic its shape, and both of these qualities enhance the dissipative effects.

Due to the relationships among the p_T spectrum, p_T averaged v_2 and p_T differential $v_2(p_T)$, the flatter the p_T spectrum, the larger the v_2 even if $v_2(p_T)$ stays the same. It is also worth noticing that the steeper the slope of $v_2(p_T)$, the larger the increase in v_2 for the same increase in mean p_T . This is the main reason why quite a similar increase of mean p_T for both MC-Glauber and MC-KLN initializations leads to much larger increase of v_2 for MC-KLN than for MC-Glauber initialization.

The initial state of the fluid dynamical expansion of heavy-ion collisions at ultrarelativistic energies is quite uncertain. This has been a longstanding issue in the physics of heavy ion collisions which must be by all means resolved. Only recently, the PHENIX Collaboration claims [37] combining analysis of v_2 and v_3 enables us to discriminate the Glauber model from the CGC model. This requires both event-by-event analysis of flow phenomenon and viscous fluid dynamics simulations, which is obviously beyond our modeling of the dynamics. From the present work, if color glass condensate (CGC) initial conditions, like the ones obtained using the MC-KLN model, are realized in nature at both RHIC and LHC energies, the larger deviation of v_2 from the data at LHC than at RHIC in Figs. 4 and 5 could mean that viscous effects are larger at LHC than at RHIC. This can indicate a larger specific shear viscosity, η/s , at larger temperatures. For a better interpretation of current experimental data, the issue should be clarified in near future by determining the initial conditions better and by a more detailed analysis using a hybrid model of viscous hydrodynamics and hadron cascade on an event-by-event basis.

4. Conclusions

In summary, we calculated transverse momentum distribution of charged hadrons, centrality dependence of integrated elliptic flow parameter v_2 and differential elliptic flow $v_2(p_T)$ in Pb+Pb collisions at $\sqrt{s_{NN}} = 2.76$ TeV and in Au+Au collisions at $\sqrt{s_{NN}} = 200$ GeV. We compared v_2 and $v_2(p_T)$ with respect to reaction plane from the hybrid model with v_2 data mainly

obtained from the 4-particle cumulant method. Transverse momentum distributions become harder, whereas the shape of $v_2(p_T)$ does not change so much as the collision energy increases. Thus the increase in p_T -integrated v_2 is due to the increase in mean p_T . However, the intrinsic slope of $v_2(p_T)$ depends on the initialization: The slope from the MC-KLN initialization is steeper than that from the MC-Glauber initialization, and thus essentially the same change of mean p_T leads to larger increase of p_T -integrated v_2 for MC-KLN initialization than for MC-Glauber initialization. The larger difference between the data and our MC-KLN result at LHC than at RHIC may indicate larger dissipative effects at LHC than at RHIC. All this emphasizes the importance of understanding initial conditions in relativistic heavy ion collisions towards extracting the bulk and transport properties of the QGP.

In future, it would be interesting to perform event-by-event hydrodynamic simulations followed by the hadronic cascade and obtain v_n in the same way as the experimental people do.

The author acknowledges the fruitful collaboration with P. Huovinen and Y. Nara. The work was partly supported by Grant-in-Aid for Scientific Research Nos. 22740151 and 22340052.

REFERENCES

- [1] J.Y. Ollitrault, *Phys. Rev.* **D46**, 229 (1992).
- [2] M. Gyulassy, arXiv:nucl-th/0403032v1.
- [3] T.D. Lee, *Nucl. Phys.* **A750**, 1 (2005); M. Gyulassy, L. McLerran, *Nucl. Phys.* **A750**, 30 (2005); E.V. Shuryak, *Nucl. Phys.* **A750**, 64 (2005).
- [4] http://www.bnl.gov/bnlweb/pubaf/pr/PR_display.asp?prID=05-38
- [5] K. Aamodt *et al.* [ALICE Collaboration], *Phys. Rev. Lett.* **105**, 252302 (2010).
- [6] G. Aad *et al.* [ATLAS Collaboration], arXiv:1108.6018v1 [hep-ex].
- [7] T. Hirano, P. Huovinen, Y. Nara, *Phys. Rev.* **C83**, 021902 (2011).
- [8] T. Hirano, P. Huovinen, Y. Nara, *Phys. Rev.* **C84**, 011901 (2011).
- [9] T. Hirano, *Phys. Rev.* **C65**, 011901 (2002); T. Hirano, K. Tsuda, *Phys. Rev.* **C66**, 054905 (2002).
- [10] Y. Nara *et al.*, *Phys. Rev.* **C61**, 024901 (2000); <http://quark.phy.bnl.gov/~ynara/jam/>
- [11] M. Cheng *et al.*, *Phys. Rev.* **D77**, 014511 (2008).
- [12] A. Bazavov *et al.*, *Phys. Rev.* **D80**, 014504 (2009).
- [13] P. Huovinen, P. Petreczky, *Nucl. Phys.* **A837**, 26 (2010).

- [14] https://wiki.bnl.gov/hhic/index.php/Lattice_calculatons_of_Equation_of_State and https://wiki.bnl.gov/TECHQM/index.php/QCD_Equation_of_State
- [15] F. Cooper, G. Frye, *Phys. Rev.* **D10**, 186 (1974).
- [16] T. Hirano *et al.*, *Phys. Rev.* **C77**, 044909 (2008).
- [17] J.D. Bjorken, *Phys. Rev.* **D27**, 140 (1983).
- [18] M.L. Miller, K. Reygers, S.J. Sanders, P. Steinberg, *Annu. Rev. Nucl. Part. Sci.* **57**, 205 (2007).
- [19] H.J. Drescher, Y. Nara, *Phys. Rev.* **C75**, 034905 (2007); *Phys. Rev.* **C76**, 041903(R) (2007); <http://www.aiu.ac.jp/~ynara/mckln/>
- [20] T. Hirano, Y. Nara, *Phys. Rev.* **C79**, 064904 (2009).
- [21] N. Borghini, P.M. Dinh, J.Y. Ollitrault, *Phys. Rev.* **C63**, 054906 (2001); *Phys. Rev.* **C64**, 054901 (2001).
- [22] S.A. Voloshin, A.M. Poskanzer, A. Tang, G. Wang, *Phys. Lett.* **B659**, 537 (2008).
- [23] J.Y. Ollitrault, A.M. Poskanzer, S.A. Voloshin, *Phys. Rev.* **C80**, 014904 (2009).
- [24] A. Adil *et al.*, *Phys. Rev.* **C74**, 044905 (2006).
- [25] P. Sorensen *et al.*, arXiv:1102.1403 [nucl-th].
- [26] D. Kharzeev, M. Nardi, *Phys. Lett.* **B507**, 121 (2001); D. Kharzeev, E. Levin, *Phys. Lett.* **B523**, 79 (2001); D. Kharzeev, E. Levin, M. Nardi, *Phys. Rev.* **C71**, 054903 (2005); *Nucl. Phys.* **A730**, 448 (2004).
- [27] S.S. Adler *et al.* [PHENIX Collaboration], *Phys. Rev.* **C69**, 034909 (2004).
- [28] T. Hirano, Y. Nara, *Nucl. Phys.* **A743**, 305 (2004).
- [29] L.V. Gribov, E.M. Levin, M.G. Ryskin, *Phys. Rep.* **100**, 1 (1983).
- [30] K. Aamodt *et al.* [ALICE Collaboration], *Phys. Rev. Lett.* **105**, 252301 (2010); *Phys. Rev. Lett.* **106**, 032301 (2011) [arXiv:1012.1657v2 [nucl-ex]].
- [31] K. Aamodt *et al.* [ALICE Collaboration], *Phys. Rev. Lett.* **106**, 032301 (2011).
- [32] K. Aamodt *et al.* [ALICE Collaboration], *Eur. Phys. J.* **C68**, 89 (2010).
- [33] T. Hirano *et al.*, *Phys. Lett.* **B636**, 299 (2006).
- [34] J. Adams *et al.* [STAR Collaboration], *Phys. Rev.* **C72**, 014904 (2005).
- [35] M. Luzum, *Phys. Rev.* **C83**, 044911 (2011).
- [36] P.F. Kolb, *Heavy Ion Phys.* **15**, 279 (2002).
- [37] A. Adare *et al.* [PHENIX Collaboration], arXiv:1105.3928 [nucl-ex].